

Virtual quantum error detection

Kento Tsubouchi^{1,*} Yasunari Suzuki² Yuuki Tokunaga² Nobuyuki Yoshioka^{1,3,4} and Suguru Endo^{2,†}

¹*Department of Applied Physics, University of Tokyo,
7-3-1 Hongo, Bunkyo-ku, Tokyo 113-8656, Japan*

²*NTT Computer and Data Science Laboratories,
NTT Corporation, Musashino, 180-8585, Tokyo, Japan*

³*Theoretical Quantum Physics Laboratory, RIKEN Cluster for Pioneering Research (CPR), Wako-shi, Saitama 351-0198, Japan*

⁴*JST, PRESTO, 4-1-8 Honcho, Kawaguchi, Saitama, 332-0012, Japan*

Quantum error correction and quantum error detection necessitate syndrome measurements to detect errors. Performing syndrome measurements for each stabilizer generator can be a significant overhead, considering the fact that the readout fidelity in the current quantum hardware is generally lower than gate fidelity. Here, by generalizing a quantum error mitigation method known as symmetry expansion, we propose a protocol called virtual quantum error detection (VQED). This method *virtually* allows for evaluating computation results corresponding to post-selected quantum states obtained through quantum error detection during circuit execution, without implementing syndrome measurements. Unlike conventional quantum error detection, which requires the implementation of Hadamard test circuits for each stabilizer generator, our VQED protocol can be performed with a constant depth shallow quantum circuit with an ancilla qubit, irrespective of the number of stabilizer generators. Furthermore, the computation results obtained using VQED are robust against the noise that occurred during the operation of VQED, and our method is fully compatible with other error mitigation schemes, enabling further improvements in computation accuracy and facilitating high-fidelity quantum computing.

I. INTRODUCTION

The last decade has seen the remarkable development of the noisy-intermediate quantum computing paradigm from both theoretical and experimental sides [1–8]. Nevertheless, the effect of noise lies as a crucial problem in realizing practical quantum computing. Quantum error correction (QEC) and quantum error detection (QED), which reduce computation errors through the encoding of logical qubits with many physical qubits, have been investigated for enhancing computation accuracy for a long time since the early days of quantum information science [9–14]. Syndrome measurements are performed in QEC and QED to detect physical errors by using ancilla qubits; QEC actively corrects physical errors based on the error information obtained in the decoding process while QED discards the noisy quantum states once an error is detected.

While the utility of QEC and QED have been shown theoretically in numerous previous works, they require high-fidelity syndrome measurements of stabilizer generators. Furthermore, the number of required syndrome measurements increases with the number of stabilizer generators in the QEC/QED code. Considering the current situation of superconducting hardware, in which the measurement fidelity is lower than gate errors [6, 15, 16], the necessity of single-shot measurements [17] for syndrome measurements can be a significant overhead in QEC/QED.

For the ease of error reduction in near-term quantum hardware, a class of error reduction techniques referred to as quantum error mitigation (QEM) has been recently studied [18–22]. In many QEM methods, the noiseless expectation values of observables are estimated via post-processing of measurement results. This indicates that we cannot physically obtain quantum states with reduced noise; nevertheless, QEM allows for *virtually* simulating the expectation values of observables for such states. Symmetry expansion (SE) is one of the QEM methods that use symmetries inherent to the system to mitigate errors [23–26]. The noisy quantum state is virtually projected onto the symmetric subspace through random sampling of the symmetry operators, additional measurements, and classical postprocessing of measurement outcomes. As we will discuss later, SE allows for the calculation of the expectation value of an observable corresponding to the post-selected quantum states through QED without implementing syndrome measurements, and hence is suitable for near-term hardware. So far, SE is theoretically formulated for error mitigation for noisy states immediately before measurement [24, 25] and state preparation for rotation symmetric bosonic codes [26]. Thus, SE in its current form cannot effectively suppress the accumulation of noise during computation, whereas the conventional QED can be more flexibly used during the circuit execution.

In this work, we significantly expand the framework of SE so that it can be leveraged during the execution of quantum algorithms. Because our method enables us to obtain the expectation values corresponding to the post-selected state via QED, we call it *virtual quantum error detection* (VQED). While the conventional SE can only detect errors immediately before the measurement of ex-

* tsubouchi@noneq.t.u-tokyo.ac.jp

† suguru.endou.uc@hco.ntt.co.jp

pectation values, VQED can detect errors even while the execution of the quantum circuit, enabling us to mitigate the accumulation of errors during the computation. Although VQED inherits the disadvantages of SE, i.e., we can only obtain error-mitigated expectation values, not the quantum state itself, and the required sampling complexity is quadratically worse for the success probability of QED, the significant advantages of VQED compared with the QED are as follows: 1. the depth for QEM is constant regardless of the number of stabilizer generators of the code; 2. we only measure an expectation value of an observable without the need for single-shot syndrome measurements; 3. the obtained expectation values are robust against the noise that occurred during the operation of VQED; 4. our method is fully compatible with other QEM methods, e.g., readout error mitigation for the ancilla qubit used in our protocol. We numerically verify the behavior of the fidelity improvement with our VQED protocol over the conventional SE and the unencoded physical qubits. We also evaluate the required sampling costs and verify that the sampling cost for VQED does not significantly increase compared to SE. Furthermore, our method can offer virtual implementation of stabilizer-like QEM methods using spin and particle number preservation in the computation [23, 27] in even more hardware-friendly manner.

In addition, we discuss the virtual implementation of quantum error correction, which results in the computation outcome corresponding to the error-corrected quantum states. While the conventional QEC does not induce additional sampling overheads, we find that our virtual QEC generally incurs a larger sampling overhead than the virtual QED method; therefore, we conclude VQED is preferred in typical quantum computation scenarios.

II. PRELIMINARIES

A. Quantum error detection and quantum error correction for stabilizer codes

We first review stabilizer codes and ways to detect and correct their errors [28, 29]. QED and QEC are performed by encoding quantum information into enlarged Hilbert space at the expense of multiple quantum systems. Due to its redundancy, we can detect and correct their errors during the computation.

Here, we review the stabilizer formalism, which is the most standard method to construct quantum error-correcting codes. Consider an n -qubit Pauli group as

$$\mathcal{G}_n = \{\pm 1, \pm i\} \times \{I, X, Y, Z\}^{\otimes n} \quad (1)$$

where I is the identity operator for single qubit system and $X = \begin{pmatrix} 0 & 1 \\ 1 & 0 \end{pmatrix}$, $Y = \begin{pmatrix} 0 & -i \\ i & 0 \end{pmatrix}$, and $Z = \begin{pmatrix} 1 & 0 \\ 0 & -1 \end{pmatrix}$ are Pauli operators. To encode k logical qubits

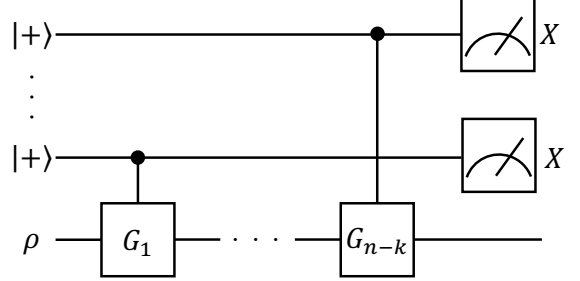


FIG. 1. Quantum circuit for quantum error detection (QED).

into n physical qubits, we define a stabilizer group $\mathcal{S} = \{S_1, \dots, S_{2^{n-k}}\} \subset \mathcal{G}_n$ as a commutative subgroup of the Pauli group \mathcal{G}_n with $-I^{\otimes N} \notin \mathcal{S}$. We denote a generator set of the stabilizer group \mathcal{S} as $\mathcal{G} = \{G_1, \dots, G_{n-k}\}$. Then, we can define the logical space of the stabilizer code \mathcal{C} as an eigenspace with $+1$ eigenvalues for all the operators in the stabilizer group, i.e., $\mathcal{C} = \{|\psi\rangle \mid \forall S_i \in \mathcal{S}, S_i |\psi\rangle = |\psi\rangle\}$. In the 2^k -dimensional Hilbert space, we can introduce a logical basis as $\{|0\rangle_L, |1\rangle_L\}^{\otimes k}$ and logical Pauli operators as $\{I_L, X_L, Y_L, Z_L\}^{\otimes k}$. The code distance d is the minimum number of physical qubits on which an arbitrary logical operator of the code non-trivially operates. We denote such stabilizer codes as $[[n, k, d]]$ stabilizer codes.

We can detect physical errors during quantum computation by measuring the generators G_1, \dots, G_{n-k} by using the Hadamard test circuits as shown in Fig 1, and such measurement is called syndrome measurement. If there exists G_i such that its measurement result is -1 , then we can determine the presence of errors during the computation. Conversely, when the measurement results are $+1$ for all G_i , we can say that there was no error with a sufficiently high probability. By continuing the computation only when the measurement results for all the generators are $+1$, we can project the noisy state $\rho = \mathcal{E}(\rho_{\text{id}})$ into the code space as

$$\rho_{\text{det}} = \frac{P\rho P}{\text{tr}[\rho P]}, \quad (2)$$

where P is a projector to the code space \mathcal{C} written as

$$P = \prod_{G_i \in \mathcal{G}} \frac{I + G_i}{2} = \frac{1}{2^{n-k}} \sum_{S_i \in \mathcal{S}} S_i. \quad (3)$$

Because the probability to measure $+1$ for all the syndrome measurements is $\text{tr}[\rho P]$, the effect of physical errors acting on less than d qubits can be eliminated with $O(\text{tr}[\rho P]^{-1})$ times more execution of quantum circuits. Note that stabilizer-like QEM methods work in a similar way when the spin and electron number preservation is imposed in the variational ansatz of quantum states [23, 27].

We can not only detect errors but also correct them by applying appropriate feedback operations according to the measurement results, enabling us to suppress the effect of noise without any additional execution of quantum circuits. When the measurement result for the generator G_i is s_i , and there is no measurement error, we can correct errors by applying a recovery operation R_s , which is estimated from $s = (s_1, \dots, s_{n-k})$ to maximize the probability of correcting erroneous quantum states to the original logical state. Since the recovery Pauli operator at least maps quantum states to a logical state, R_s commutes with G_i if $s_i = +1$ and anti-commutes if $s_i = -1$. In this way, the effect of physical errors acting on less than $\lfloor (d-1)/2 \rfloor$ qubits can be corrected as

$$\rho_{\text{cor}} = \sum_{s \in \{-1,1\}^{n-k}} E_s \rho E_s, \quad (4)$$

where

$$\begin{aligned} E_s &= R_s \prod_i \frac{I + s_i G_i}{2} \\ &= P R_s. \end{aligned} \quad (5)$$

While QEC and QED can reduce the effective error rates, they impose additional difficulties in the implementation. To implement QEC and QED, we need repetitive applications of Pauli measurements for all the elements in the stabilizer generator set. Since the error rates of measurement operations are typically higher than the others [6, 15, 16], they induce large overheads on the process. In the case of QEC, we also need to estimate recovery operations from the observed syndrome values, and error rates must be smaller than the value called code threshold for a reliable estimation.

B. Symmetry expansion

In order to combat errors on near-term devices, QEM has been developed in recent years [21, 22]. Symmetry expansion (SE) is one of the promising QEM methods which mitigates errors by virtually projecting the noisy quantum state onto the symmetric subspace without syndrome measurements [24, 25].

Suppose that we want to estimate an expectation value of an observable O for a noiseless state ρ_{id} from the measurement of the noisy state $\rho = \mathcal{E}(\rho_{\text{id}})$. We assume that the observable O commutes with the projector P . Then, we can mitigate errors by virtually projecting the noisy states onto the code space as

$$\begin{aligned} \text{tr}[\rho_{\text{det}} O] &= \frac{\text{tr}[\rho O P]}{\text{tr}[\rho P]} \\ &= \frac{2^{-(n-k)} \sum_{S_i \in \mathcal{S}_i} \text{tr}[\rho O S_i]}{2^{-(n-k)} \sum_{S_i \in \mathcal{S}_i} \text{tr}[\rho S_i]}, \end{aligned} \quad (6)$$

which can be calculated in the following way.

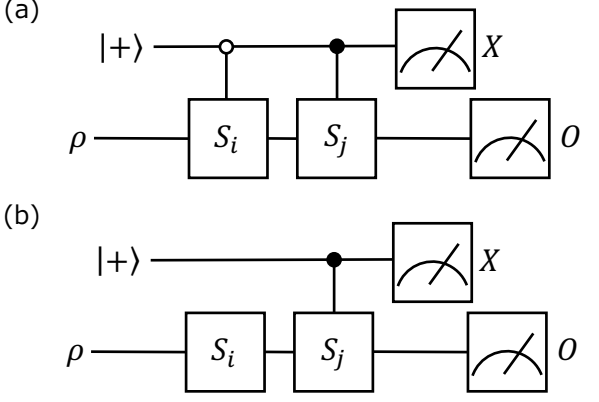


FIG. 2. Quantum circuits for virtually projecting a quantum state ρ into the code space. The white/black circles indicate the control operations which act for the state 0/1. The circuit in Panel (a) utilizes two controlled-stabilizer gates, whereas the circuit in Panel (b) can virtually project quantum states using only a single controlled-stabilizer gate.

1. For $s = 1, \dots, N$, repeat the following operations.
 - (a) Uniformly sample $S_i \in \mathcal{S}$.
 - (b) Simultaneously measure the noisy state ρ for S_i and OS_i , and record the results as a_s and b_s .
2. Calculate $a = \frac{1}{N} \sum_s a_s$ and $b = \frac{1}{N} \sum_s b_s$.
3. Output b/a .

The number of measurements needed to estimate Eq. (6) for some fixed accuracy ε is known to scale as $N = O(\varepsilon^{-2} \text{tr}[\rho P]^{-2})$. In this way, we can obtain an error-mitigated expectation value of the observable O , which corresponds to the virtual projection of the noisy state immediately before the measurement ρ onto ρ_{det} .

III. VIRTUAL QUANTUM ERROR DETECTION

Symmetry expansion is only applicable to the state immediately before measurement [24, 25] and state preparation for rotation symmetric bosonic codes [26]. In this section, we introduce our VQED method, which allows for the computation of error-mitigated expectation values corresponding to the post-selected states after syndrome measurements during circuit execution.

Let us first explain the way to virtually project a quantum state ρ into the code space by using the circuit shown in Fig. 2 (a). We can derive the expectation value obtained through this circuit as:

$$\frac{1}{2} (\text{tr}[S_i \rho S_j O] + \text{tr}[S_j \rho S_i O]). \quad (7)$$

Thus, by uniformly sampling $i, j \in \{1, \dots, 2^{n-k}\}$ and taking the average of the distribution, we can obtain the expectation value of the projected state as

$$\text{tr}[P\rho PO] \quad (8)$$

since the average of S_i can be written as $\langle S_i \rangle = 2^{-(n-k)} \sum_i S_i = P$.

We can further simplify the circuit as in Fig. 2 (b) for stabilizer codes. The expectation value obtained through this circuit is

$$\frac{1}{2}(\text{tr}[S_j S_i \rho S_i O] + \text{tr}[S_i \rho S_i S_j O]). \quad (9)$$

Thus, by uniformly sampling $i, j \in \{1, \dots, 2^{n-k}\}$ and taking the average of the distribution, we can also obtain Eq. (8) since $PS_i = S_iP = P$ holds.

These methods can be used to virtually detect errors in noisy quantum circuits. We consider a logical quantum circuit composed of a state preparation of a logical initial state ρ_0 followed by L logical unitary gate $\mathcal{U}_l(\cdot) = U_l \cdot U_l^\dagger$ ($l = 1, \dots, L$), and a measurement of an observable O in the hope of estimating the expectation value of O for the state $\rho_{\text{id}} = \mathcal{U}_L \circ \dots \circ \mathcal{U}_1(\rho_0)$. However, we assume that these logical quantum gates are affected by Markovian noise and that the actual gates are represented as $\mathcal{U}'_l = \mathcal{E}_l \circ \mathcal{U}_l$. For simplicity, we ignore state preparation and measurement (SPAM) errors, but these effects can easily be reflected. When we can perform quantum error detection after each gate, we will have

$$\rho_{\text{det}} = \frac{\rho'_{\text{det}}}{\text{tr}[\rho'_{\text{det}}]}, \quad (10)$$

where

$$\rho'_{\text{det}} = \mathcal{P} \circ \mathcal{E}_L \circ \mathcal{U}_L \circ \dots \circ \mathcal{P} \circ \mathcal{E}_1 \circ \mathcal{U}_1(\rho_0). \quad (11)$$

Here, we define $\mathcal{P}(\cdot) = P \cdot P$.

In order to obtain the expectation value for ρ_{det} through VQED, we construct a quantum circuit represented in Fig. 3. This circuit allows for computing the expectation values corresponding to the error-detection circuits by performing S_{i_l} gate on the noisy circuit, preparing a single qubit ancilla initialized to $|+\rangle$, coupling the ancilla qubit with the noisy circuit through controlled- S_{j_l} gate, and measuring the ancilla in the X bases. Note that the frequency of applying these operation for VQED can be reduced according to the noise level, although we discuss gate-wise VQED for generality. The state immediately before the measurement of this circuit ρ_{bf} reads:

$$\begin{aligned} \rho_{\text{bf}} &= \frac{1}{2^L} \sum_{\mathbf{pq}} |\mathbf{p}\rangle \langle \mathbf{q}| \otimes \rho_{ij}^{\mathbf{pq}}, \\ \rho_{ij}^{\mathbf{pq}} &= \mathcal{P}_{i_L j_L}^{p_L q_L} \circ \mathcal{E}_L \circ \mathcal{U}_L \circ \dots \circ \mathcal{P}_{i_1 j_1}^{p_1 q_1} \circ \mathcal{E}_1 \circ \mathcal{U}_1(\rho_0), \end{aligned} \quad (12)$$

where \mathbf{p} and \mathbf{q} are bitstrings of length L and

$$\mathcal{P}_{i_l j_l}^{p_l q_l}(\cdot) = S_{j_l}^{p_l} S_{i_l} \cdot S_{i_l} S_{j_l}^{q_l}. \quad (13)$$

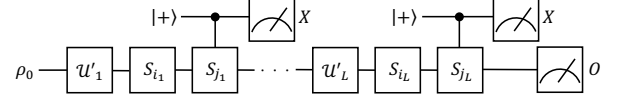


FIG. 3. Quantum circuit for virtual quantum error detection (VQED).

Then, the expectation value of the observable $X^{\otimes L} \otimes O$ in this state is:

$$\begin{aligned} \langle X^{\otimes L} \otimes O \rangle &= \text{tr}[\rho_{\text{bf}} X^{\otimes L} \otimes O] \\ &= \frac{1}{2^L} \sum_{\mathbf{p}} \text{tr}[\rho_{ij}^{\mathbf{pp}+1} O] \end{aligned} \quad (14)$$

where $\mathbf{1}$ is a bit string of length L whose elements are all 1. When we uniformly sample $i_l, j_l \in \{1, \dots, 2^{n-k}\}$ ($1 \leq l \leq L$) and denote the expectation value under the probability distribution as $\langle \cdot \rangle_{ij}$, we can project the noisy state into the code space after each noisy gate as

$$\begin{aligned} \langle \rho_{ij}^{\mathbf{pp}+1} \rangle_{ij} &= \mathcal{P} \circ \mathcal{E}_L \circ \mathcal{U}_L \circ \dots \circ \mathcal{P} \circ \mathcal{E}_1 \circ \mathcal{U}_1(\rho_0) \\ &= \rho'_{\text{det}}, \end{aligned} \quad (15)$$

where we use

$$\begin{aligned} \langle \mathcal{P}_{i_l j_l}^{p_l p_l+1}(\cdot) \rangle_{i_l j_l} &= \langle S_{j_l}^{p_l} S_{i_l} \cdot S_{i_l} S_{j_l}^{1-p_l} \cdot \rangle_{i_l j_l} \\ &= \begin{cases} \langle S_{i_l} \cdot S_{i_l} S_{j_l} \rangle_{i_l j_l} & (p_l = 0) \\ \langle S_{j_l} S_{i_l} \cdot S_{i_l} \rangle_{i_l j_l} & (p_l = 1) \end{cases} \\ &= P \cdot P. \end{aligned} \quad (16)$$

Thus, the expectation value of the observable O for the post-selected state ρ_{det} can be represented as:

$$\text{tr}[\rho_{\text{det}} O] = \frac{\left\langle \text{tr} \left[\left(\frac{1}{2^L} \sum_{\mathbf{pq}} |\mathbf{p}\rangle \langle \mathbf{q}| \otimes \rho_{ij}^{\mathbf{pq}} \right) X^{\otimes L} \otimes O \right] \right\rangle_{ij}}{\left\langle \text{tr} \left[\left(\frac{1}{2^L} \sum_{\mathbf{pq}} |\mathbf{p}\rangle \langle \mathbf{q}| \otimes \rho_{ij}^{\mathbf{pq}} \right) X^{\otimes L} \otimes I \right] \right\rangle_{ij}}. \quad (17)$$

Therefore, we can perform our VQED in the noisy quantum circuit with the following procedure:

1. For $s = 1, \dots, N$, repeat the following operation.
 - (a) Uniformly sample $i_l, j_l \in \{1, \dots, 2^{n-k}\}$ ($1 \leq l \leq L$).
 - (b) Run the circuit illustrated in Fig. 3.
 - (c) Record the product of the X measurement as a_s and the product of a_s and O measurement as b_s .
2. Calculate $a = \frac{1}{N} \sum_s a_s$ and $b = \frac{1}{N} \sum_s b_s$.
3. Output b/a .

In this way, with the sampling overhead of $N = O(\varepsilon^{-2} \text{tr}[\rho'_{\text{det}}]^{-2})$, we can perform VQED to virtually

(a) [[4, 1, 2]] stabilizer code		(b) [[5, 1, 3]] stabilizer code		(c) [[7, 1, 3]] stabilizer code	
Name	Operator	Name	Operator	Name	Operator
G_1	$XXXX$	G_1	$XZZXI$	G_1	$IIIZZZZ$
G_2	$ZZZZ$	G_2	$IXZZX$	G_2	$IZZIIZZ$
G_3	$IZZI$	G_3	$XIXZZ$	G_3	$ZIZIZIZ$
Z_L	$ZZII$	G_4	$ZXIXZ$	G_1	$IIIXXXX$
X_L	$IXXI$	Z_L	$ZZZZZ$	G_2	$IXXIIXX$
		X_L	$XXXXX$	G_3	$XIXIXIX$

TABLE I. Generators and logical operators for (a) [[4, 1, 2]], (b) [[5, 1, 3]], and (c) [[7, 1, 3]] stabilizer codes.

detect errors that occurred during the computation with some fixed accuracy (standard deviation) ε . Note that while we focus on the stabilizer QEC/QED codes, our method can be straightforwardly applied to the stabilizer-based QEM method for the spin and electron number preservation [23, 27] for more near-term quantum hardware.

Note that our VQED protocol circumvents the syndrome measurements of stabilizer generators that need high-fidelity single-shot measurement of ancilla qubits; our method only measures expectation values of the observable. Moreover, while quantum error detection requires measurements of $n - k$ stabilizer generators via Hadamard test circuits shown in Fig. 1, our method only necessitates a single controlled operations irrespective of the number of stabilizer generators.

Furthermore, the obtained expectation value is robust against noise that occurs in the ancilla qubit. Since we calculate the expectation value of X for each ancilla, the only terms of the ancilla that affect Eq. (17) are $|0\rangle\langle 1|$ and $|1\rangle\langle 0|$. Thus, even if the single qubit depolarizing noise $\mathcal{E}_p : \rho \mapsto (1-p)\rho + pI/2$ affects each ancilla during the execution of controlled- S_{j_l} gate, the numerator and the denominator of Eq. (17) are only multiplied by $(1-p)^L$. Therefore, the value obtained through VQED remains unchanged. Note that this is also the case even when we consider the circuit level noise where each CNOT gate and CZ gate to implement the controlled- S_{j_l} is affected by single qubit depolarizing noise, since the noisy term represented as $|0\rangle\langle 0| \otimes \rho + |1\rangle\langle 1| \otimes \rho'$, where ρ and ρ' are the state of the system qubits where noise may be propagated, is canceled out when we take the expectation value of X . The same principle applies to other noise models which are not biased by Pauli X or Y , such as local dephasing and amplitude damping noise. We further discuss these points in Appendix A. We also want to mention that, by combining the readout error mitigation method with our method for the ancilla qubits, we can perform high-fidelity virtual projection onto the code space even under the existence of measurement errors.

The disadvantages of VQED are that we can only obtain the error-mitigated expectation values, not the quantum state itself as well as quadratically worse sampling cost for the projection probability $\text{tr}[\rho'_{\text{det}}]$. While sampling costs can only be overcome by increased paralleliza-

tion, lightweight quantum phase estimation algorithms only employing expectation values are proposed [30–33] in addition to the fact that most of NISQ algorithms use expectation values. Our VQED methods can be used in such algorithms.

IV. VIRTUAL IMPLEMENTATION OF QUANTUM ERROR CORRECTION

We also discuss how to perform quantum error correction virtually without any syndrome measurements and feedback operations. The main idea is that the error-corrected state as in Eq. (4) can be also written as

$$\rho_{\text{cor}} = \sum_{\mathbf{s} \in \{-1, 1\}^{n-k}} \mathcal{P}(R_{\mathbf{s}} \rho R_{\mathbf{s}}). \quad (18)$$

Thus, we can virtually correct errors by uniformly sampling $s_1, \dots, s_{n-k} \in \{+1, -1\}$, applying $R_{\mathbf{s}}$ to the noisy state, virtually projecting the state into the codespace using the way mentioned above, and multiplying the result by 2^{n-k} . However, the sampling cost of this method scales as $2^{2(n-k)}$, which grows exponentially with the number of redundant qubits. We may decrease the cost by limiting the scope of the sum. Let $B \subset \{-1, 1\}^n$ be a subset of highly probable measurement results such as the measurement results when an error did not occur or occurred only once. Then, we may approximate the error-corrected state as

$$\rho_{\text{cor}'} = \frac{1}{\sum_{\mathbf{s} \in B} p_{\mathbf{s}}} \sum_{\mathbf{s} \in B} \mathcal{P}(R_{\mathbf{s}} \rho R_{\mathbf{s}}) \quad (19)$$

where $p_{\mathbf{s}} = \text{tr}[PR_{\mathbf{s}} \rho R_{\mathbf{s}}]$ represents the probability of obtaining \mathbf{s} at the syndrome measurement. However, the sampling cost of virtually calculating this state is $|B|^2(1/\sum_{\mathbf{s} \in B} p_{\mathbf{s}})^2$, which is still significantly higher than just performing VQED with $B = \{1\}^n$. Furthermore, while error detection can detect errors of at most d qubits, error correction can only correct errors of at most $\lfloor (d-1)/2 \rfloor$ qubits. This means that even the accuracy of this virtual implementation of QEC is generally worse than VQED. Even though these methods may be more effective than VQED in the case where the noise maps

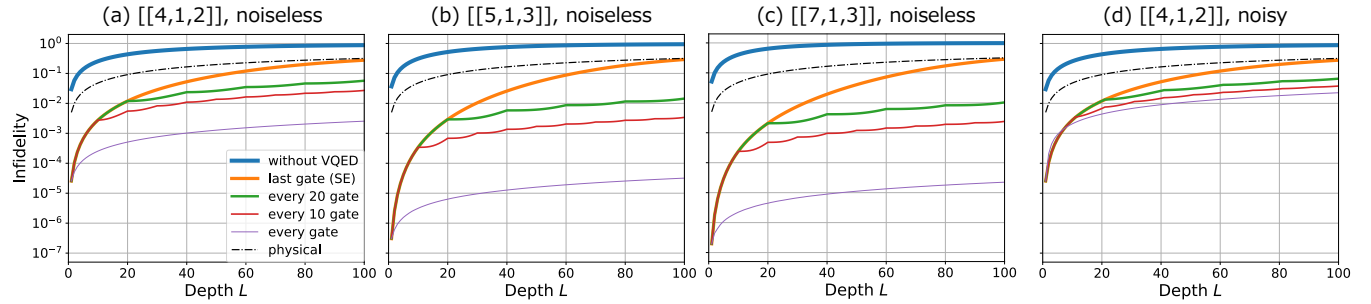


FIG. 4. Depth L dependence of infidelity $1 - \text{tr}[\rho_{\text{det}} |\bar{\Psi}\rangle\langle \bar{\Psi}|] = 1 - \langle \bar{\Psi} | \rho_{\text{det}} | \bar{\Psi} \rangle$ between the output state of the noisy circuit with VQED ρ_{det} and the noiseless circuit $|\bar{\Psi}\rangle$ for (a) and (d): $[[4, 1, 2]]$, (b): $[[5, 1, 3]]$, and (c): $[[7, 1, 3]]$ stabilizer codes. Panels (a)-(c) denotes the results when the controlled-stabilizer gates are noiseless and (d) denotes the results when the VQED gadgets are affected by local depolarizing noise. The “without VQED” line represents infidelity when we did not perform VQED. The “last gate (SE)” line represents infidelity when we perform VQED only before the measurement, which is just a normal SE, as in Refs. [24, 25]. The “every 20 gates” and the “every 10 gates” lines represent infidelity when we perform VQED after every 20 and 10 gates. The “every gate” line represents infidelity when we perform VQED after every gate. The “physical” line represents the infidelity of a single physical qubit without encoding.

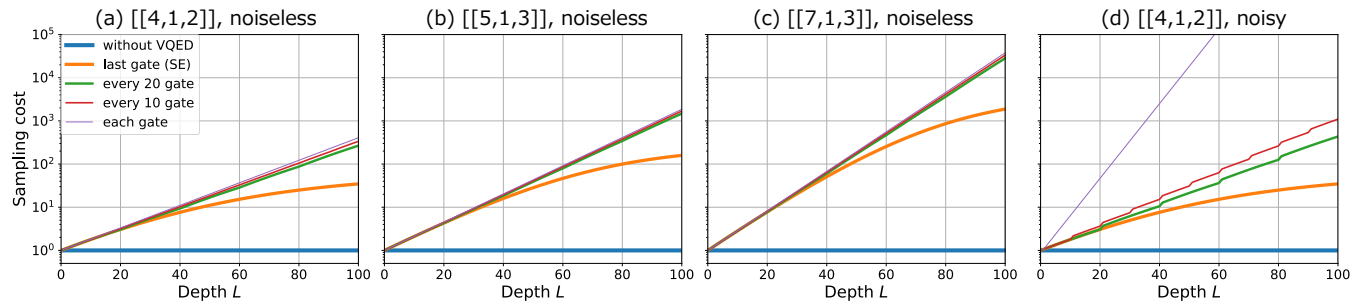


FIG. 5. Scaling of the sampling cost $\text{tr}[\rho'_{\text{det}}]^{-2}$ with respect to the depth L of the quantum circuit for (a) and (d): $[[4, 1, 2]]$, (b): $[[5, 1, 3]]$, and (c): $[[7, 1, 3]]$ stabilizer codes. Panels (a)-(c) denotes the results when the VQED gadgets are noiseless and (d) denotes the results when the VQED gadgets are affected by local depolarizing noise. The “without VQED” line represents sampling cost when we did not perform VQED. The “last gate (SE)” line represents sampling cost when we perform VQED only before the measurement, which is just a normal SE, as in Refs. [24, 25]. The “every 20 gates” and the “every 10 gates” lines represent the sampling cost when we perform VQED after every 20 and 10 gates. The “every gate” line represents the sampling cost when we perform VQED after every gate.

the state in the code space outside of it with high probability, finding practical scenarios to utilize these methods is left as our future work.

V. NUMERICAL SIMULATION

In this section, we numerically evaluate the performance of our method for $[[4, 1, 2]]$, $[[5, 1, 3]]$, and $[[7, 1, 3]]$ stabilizer codes [11, 12, 14]. The generators and logical operators of these codes are shown in Tabel I. Similar to the numerical calculation presented in the previous study on SE [24], we initialize the state ρ_0 as the logical state $|0\rangle_L$, and the unitary gate U_l is randomly chosen from a set of transversal single-qubit gates [29, 34]. We specify the set of transversal single-qubit gates we use in Appendix B. We assume that the local depolarizing noise $\mathcal{E} = \mathcal{E}_p^{\otimes n}$ ($\mathcal{E}_p(\rho) = (1 - np)\rho + pI/2$) disturb

the circuit with noise strength $p = 0.01$ each after the gate. We numerically calculate the depth L dependence of the infidelity $1 - \langle \bar{\Psi} | \rho_{\text{det}} | \bar{\Psi} \rangle$ between the output state of the noisy circuit ρ_{det} and the noiseless circuit $|\bar{\Psi}\rangle$, and the scaling of the sampling cost $\text{tr}[\rho'_{\text{det}}]^{-2}$ by using QuTiP [35].

Our results are shown in Fig. 4 and Fig. 5. As shown in Fig. 4, we can reduce the infidelity using VQED compared to a single physical qubit affected by the error \mathcal{E}_p without encoding. Furthermore, frequent application of VQED during the circuit execution prevents the noisy state to be highly mixed on the code space. This allows us to suppress logical errors that cannot be mitigated by the conventional SE performed only on the state immediately before the measurement [24, 25]. We also find that we can reduce infidelity without performing error detection after every gate: we can sufficiently mitigate errors simply by performing VQED after every fixed number of

gates. This fact can be useful when the measurement time is much longer than the gate execution time. By comparing infidelity among different codes, we can say that infidelity becomes smaller as the code distance gets larger.

Fig. 5 shows that the sampling cost increases exponentially with the circuit depth L when we perform VQED frequently. This scaling can be roughly considered to be given by the square inverse of the probability that a state in the code space remains in the code space when the noise is applied; thus we can say $N \sim \text{tr}[\rho'_{\text{det}}]^{-2} = O((1 - \frac{3}{4}p)^{-2nL})$. It is noteworthy that the sampling cost is not significantly influenced by the frequency of VQED, even when comparing the cases of the conventional SE and VQED applied each after the gate (See the numerical results up to the depth $L = 40$, for example). Meanwhile, it may appear that the sampling cost of SE approaches a constant value for large L . However, this is because the accumulated errors increase and the noisy state approaches a completely mixed state, and thus the sampling cost converges to $N \sim \text{tr}[I/2^n P] = \frac{1}{2^{n-k}}$.

In Fig. 4 (d) and Fig. 5 (d), we also present the performance of VQED for $[[4, 1, 2]]$ stabilizer code when the VQED gadgets S_{i_l} gate and controlled- S_{j_l} gate in Fig. 3 are each affected by the local depolarizing noise $\mathcal{E}_p^{\otimes n}$ and $\mathcal{E}_p^{\otimes(n+1)}$ with the same error rate $p = 0.01$. See Appendix C for the results for $[[5, 1, 3]]$ and $[[7, 1, 3]]$ stabilizer codes. In the previous section, we have mentioned that a wide class of realistic noise that occurred in the ancilla does not affect the accuracy of VQED. By comparing Fig. 4 (a) and Fig. 4 (d), we can also say that even in the presence of additional noise acting on the system qubits, VQED still significantly outperforms the unmitigated results and the conventional SE. Meanwhile, we can see from Fig. 5 (a) and Fig. 5 (d) that the sampling cost increases when we assume that the noise affects the VQED gadget. This is mainly because the probability that a state in the code space remains in the space decreases due to the additional noise acting on the system qubits, and the denominator in Eq. (17) is multiplied by the factor of $(1 - p)^L$. Thus, the sampling cost scales as $N \sim O((1 - \frac{3}{4}p)^{-6nL}(1 - p)^{-2L})$. However, these effects can be circumvented by reducing the frequency of applying the operation of VQED.

From the above, we can say that our method can be used effectively by adjusting the code distance or frequency of VQED according to the hardware constraints, the desired accuracy, or the allowable sampling cost.

VI. DISCUSSION

We propose virtual quantum error detection (VQED) so that the computation errors during the circuit execution can be flexibly suppressed by using additional two-qubit operations and measurements in the X basis. We verify in the numerical simulations that our virtual quantum error detection protocol allows for the realization

of significantly higher-fidelity calculation of expectation values, compared with the conventional symmetry expansion method, at the cost of sampling costs. We also discuss the virtual implementation of quantum error correction; however, even though the fidelity of the quantum state after quantum error correction is generally lower than that for quantum error detection, the sampling cost of virtual implementation of quantum error correction becomes larger than VQED.

Although we mainly discuss the stabilizer codes based on the Pauli group, we can apply our method to other types of codes such as rotation symmetric bosonic codes (RSBCs) [36] as well. In Ref. [26], symmetry expansion in RSBCs is proposed, but it is restricted to state preparation and immediately before measurement. By considering the rotation symmetry operators rather than Pauli symmetries, we can also perform virtual quantum error detection for RSBCs, which is a significant generalization of Ref. [26]. In this case, we need controlled-rotation gates, which is implemented by the dispersive interactions [37] between the resonator and the ancilla qubit.

Even after the application of VQED, there remains a finite logical error, e.g., due to the limitations of code distances. Therefore, the efficient combination of VQED with other QEM methods, e.g, purification-based QEM [38–43], will also be an important research direction for the realization of even more accurate quantum computing. Also, because VQED can be regarded as a QEM method implemented on the code space, the relationship between VQED and other hybrid QEM/QEC methods are worth exploring [30, 44–46].

Experimental implementation of VQED is also an important direction for future work. The VQED circuit we propose in Fig. 3 requires connectivity between the ancilla qubit and all the qubits constructing logical qubits, and we generally need swap operations to implement controlled-stabilizer operations in the case of restricted connectivity, e.g., current superconducting hardware. However, we can relax the requirement by assigning different ancilla qubits for each logical qubit and flexibly choosing the arrangement of the ancilla qubits according to the constraints of the experiment. For example, for trapped ion systems, all-to-all connectivity is a relatively reasonable assumption [47]; therefore, one ancilla qubits may be iteratively used for all logical qubits. Meanwhile, superconducting qubit devices have restricted connectivity [6], and it may be better to assign different ancilla qubits to each logical qubit.

Finally, information-theoretic analysis of QEM is one of the intensively studied topic [48–53]. As far as we know, symmetries of the system is not explicitly considered in these works while our work shows that they can play a crucial role for QEM. Therefore, the construction of an information-theoretic analysis of QEM incorporating the symmetries may shed light on e.g., the characterization cost of the noise model for performing QEM.

ACKNOWLEDGMENTS

This work is supported by PRESTO, JST, Grant No. JPMJPR1916, JPMJPR2114, JPMJPR2119; CREST, JST, Grant No. JPMJCR1771; MEXT Q-LEAP

Grant No. JPMXS0120319794 and JPMXS0118068682, JST Moonshot R&D, Grant No. JPMJMS2061, and COI-NEXT program Grant No. JPMJPF2221. K.T. is supported by Worldleading Innovative Graduate Study Program for Materials Research, Industry, and Technology (MERITWINGS) of the University of Tokyo.

[1] J. Preskill, *Quantum* **2**, 79 (2018).

[2] S. McArdle, S. Endo, A. Aspuru-Guzik, S. C. Benjamin, and X. Yuan, *Reviews of Modern Physics* **92**, 015003 (2020).

[3] M. Cerezo, A. Arrasmith, R. Babbush, S. C. Benjamin, S. Endo, K. Fujii, J. R. McClean, K. Mitarai, X. Yuan, L. Cincio, *et al.*, *Nature Reviews Physics* **3**, 625 (2021).

[4] J. Tilly, H. Chen, S. Cao, D. Picozzi, K. Setia, Y. Li, E. Grant, L. Wossnig, I. Rungger, G. H. Booth, *et al.*, *Physics Reports* **986**, 1 (2022).

[5] K. Bharti, A. Cervera-Lierta, T. H. Kyaw, T. Haug, S. Alperin-Lea, A. Anand, M. Degroote, H. Heimonen, J. S. Kottmann, T. Menke, *et al.*, arXiv preprint arXiv:2101.08448 (2021).

[6] F. Arute, K. Arya, R. Babbush, D. Bacon, J. C. Bardin, R. Barends, R. Biswas, S. Boixo, F. G. Brandao, D. A. Buell, *et al.*, *Nature* **574**, 505 (2019).

[7] A. Kandala, A. Mezzacapo, K. Temme, M. Takita, M. Brink, J. M. Chow, and J. M. Gambetta, *Nature* **549**, 242 (2017).

[8] L. S. Madsen, F. Laudenbach, M. F. Askarani, F. Rortais, T. Vincent, J. F. Bulmer, F. M. Miatto, L. Neuhaus, L. G. Helt, M. J. Collins, *et al.*, *Nature* **606**, 75 (2022).

[9] S. J. Devitt, W. J. Munro, and K. Nemoto, *Reports on Progress in Physics* **76**, 076001 (2013).

[10] D. A. Lidar and T. A. Brun, *Quantum error correction* (Cambridge university press, 2013).

[11] M. Grassl, T. Beth, and T. Pellizzari, *Physical Review A* **56**, 33 (1997).

[12] A. M. Steane, *Physical Review Letters* **77**, 793 (1996).

[13] P. W. Shor, *Physical review A* **52**, R2493 (1995).

[14] R. Laflamme, C. Miquel, J. P. Paz, and W. H. Zurek, *Physical Review Letters* **77**, 198 (1996).

[15] R. Hicks, B. Kobrin, C. W. Bauer, and B. Nachman, *Physical Review A* **105**, 012419 (2022).

[16] J. M. Günther, F. Tacchino, J. R. Wootton, I. Tavernelli, and P. K. Barkoutsos, *Quantum Science and Technology* **7**, 015009 (2021).

[17] In this work, we use the term “single-shot measurement” to represent the measurements that are performed only once, rather than repeating the measurement many times in order to obtain the expectation value of some observable. Note that the meaning is different from the term “single-shot error correction” [54].

[18] K. Temme, S. Bravyi, and J. M. Gambetta, *Physical review letters* **119**, 180509 (2017).

[19] Y. Li and S. C. Benjamin, *Physical Review X* **7**, 021050 (2017).

[20] S. Endo, S. C. Benjamin, and Y. Li, *Physical Review X* **8**, 031027 (2018).

[21] S. Endo, Z. Cai, S. C. Benjamin, and X. Yuan, *Journal of the Physical Society of Japan* **90**, 032001 (2021).

[22] Z. Cai, R. Babbush, S. C. Benjamin, S. Endo, W. J. Huggins, Y. Li, J. R. McClean, and T. E. O’Brien, arXiv preprint arXiv:2210.00921 (2022).

[23] X. Bonet-Monroig, R. Sagastizabal, M. Singh, and T. O’Brien, *Physical Review A* **98**, 062339 (2018).

[24] J. R. McClean, Z. Jiang, N. C. Rubin, R. Babbush, and H. Neven, *Nature communications* **11**, 1 (2020).

[25] Z. Cai, *Quantum* **5**, 548 (2021).

[26] S. Endo, Y. Suzuki, K. Tsubouchi, R. Asaoka, K. Yamamoto, Y. Matsuzaki, and Y. Tokunaga, arXiv preprint arXiv:2211.06164 (2022).

[27] S. McArdle, X. Yuan, and S. Benjamin, *Physical review letters* **122**, 180501 (2019).

[28] M. A. Nielsen and I. Chuang, “Quantum computation and quantum information,” (2002).

[29] D. Gottesman, *Stabilizer codes and quantum error correction* (California Institute of Technology, 1997).

[30] Y. Suzuki, S. Endo, K. Fujii, and Y. Tokunaga, *PRX Quantum* **3**, 010345 (2022).

[31] L. Lin and Y. Tong, *PRX Quantum* **3**, 010318 (2022).

[32] K. Wan, M. Berta, and E. T. Campbell, *Physical Review Letters* **129**, 030503 (2022).

[33] R. Zhang, G. Wang, and P. Johnson, *Quantum* **6**, 761 (2022).

[34] D. Gottesman, arXiv preprint arXiv:1610.03507 (2016).

[35] J. R. Johansson, P. D. Nation, and F. Nori, *Computer Physics Communications* **183**, 1760 (2012).

[36] A. L. Grimsmo, J. Combes, and B. Q. Baragiola, *Physical Review X* **10**, 011058 (2020).

[37] A. Blais, A. L. Grimsmo, S. M. Girvin, and A. Wallraff, *Reviews of Modern Physics* **93**, 025005 (2021).

[38] W. J. Huggins, S. McArdle, T. E. O’Brien, J. Lee, N. C. Rubin, S. Boixo, K. B. Whaley, R. Babbush, and J. R. McClean, *Physical Review X* **11**, 041036 (2021).

[39] B. Koczor, *Physical Review X* **11**, 031057 (2021).

[40] M. Huo and Y. Li, *Physical Review A* **105**, 022427 (2022).

[41] N. Yoshioka, H. Hakoshima, Y. Matsuzaki, Y. Tokunaga, Y. Suzuki, and S. Endo, *Physical Review Letters* **129**, 020502 (2022).

[42] A. Seif, Z.-P. Cian, S. Zhou, S. Chen, and L. Jiang, *PRX Quantum* **4**, 010303 (2023).

[43] T. E. O’Brien, S. Polla, N. C. Rubin, W. J. Huggins, S. McArdle, S. Boixo, J. R. McClean, and R. Babbush, *PRX Quantum* **2**, 020317 (2021).

[44] Y. Xiong, D. Chandra, S. X. Ng, and L. Hanzo, *IEEE Access* **8**, 228967 (2020).

[45] C. Piveteau, D. Sutter, S. Bravyi, J. M. Gambetta, and K. Temme, *Physical Review Letters* **127**, 200505 (2021).

[46] M. Lostaglio and A. Ciani, *Physical Review Letters* **127**, 200506 (2021).

- [47] C. Figgatt, A. Ostrander, N. M. Linke, K. A. Landsman, D. Zhu, D. Maslov, and C. Monroe, *Nature* **572**, 368 (2019).
- [48] R. Takagi, *Physical Review Research* **3**, 033178 (2021).
- [49] R. Takagi, S. Endo, S. Minagawa, and M. Gu, *npj Quantum Information* **8**, 114 (2022).
- [50] R. Takagi, H. Tajima, and M. Gu, *arXiv preprint arXiv:2208.09178* (2022).
- [51] K. Tsubouchi, T. Sagawa, and N. Yoshioka, *arXiv preprint arXiv:2208.09385* (2022).
- [52] H. Hakoshima, Y. Matsuzaki, and S. Endo, *Physical Review A* **103**, 012611 (2021).
- [53] Y. Quek, D. S. França, S. Khatri, J. J. Meyer, and J. Eisert, *arXiv preprint arXiv:2210.11505* (2022).
- [54] H. Bombín, *Physical Review X* **5**, 031043 (2015).

Appendix A: Robustness against the noise in ancilla qubits

In this section, we discuss the robustness of the VQED gadget against the noise in ancilla qubits. In order to perform S_i or controlled- S_j gates in the VQED gadget, we need to perform Pauli or controlled-Pauli gates as in Fig. 6. Here, let us assume that the ancilla qubit is noisy and affected by the single-qubit depolarizing noise $\mathcal{E}_p : \rho \mapsto (1-p)\rho + pI/2$ every time we perform controlled-Pauli gates. If the error occurred on the controlled-Pauli gates, the error propagates to the system qubits and may cause an undetectable error. This may seem to ruin the performance of VQED. However, our VQED protocol is not based on single-shot stabilizer measurements that are highly sensitive to such noise; our method only measures the expectation value of observables, and thus the effect of the error on the ancilla qubits can be removed.

When we apply the noisy VQED gadget as in Fig. 6 to the state ρ , the state before the measurement will be

$$\frac{(1-p)^{w(S_j)}}{2} (|0\rangle\langle 0| \otimes S_i \rho S_i + |1\rangle\langle 1| \otimes S_j S_i \rho S_i S_j + |1\rangle\langle 0| \otimes S_j S_i \rho S_i + |0\rangle\langle 1| \otimes S_i \rho S_i S_j + |0\rangle\langle 0| \otimes \rho' + |1\rangle\langle 1| \otimes \rho''), \quad (\text{A1})$$

where $w(S_j)$ is the Pauli weight of S_j (the number of Pauli operator in S_j) and ρ' and ρ'' are unnormalized noisy quantum states in the system qubits. By inserting additional noise in the ancilla qubits before the measurement, we can further convert this state to

$$\frac{(1-p)^n}{2} (|0\rangle\langle 0| \otimes S_i \rho S_i + |1\rangle\langle 1| \otimes S_j S_i \rho S_i S_j + |1\rangle\langle 0| \otimes S_j S_i \rho S_i + |0\rangle\langle 1| \otimes S_i \rho S_i S_j + |0\rangle\langle 0| \otimes \rho''' + |1\rangle\langle 1| \otimes \rho'''), \quad (\text{A2})$$

where ρ''' and ρ'''' are also unnormalized noisy quantum states in the system qubits. When we take the expectation value of the operator $X \otimes O$ for this state, we obtain

$$\frac{(1-p)^n}{2} (\text{tr}[S_j S_i \rho S_i O] + \text{tr}[S_i \rho S_i S_j O]), \quad (\text{A3})$$

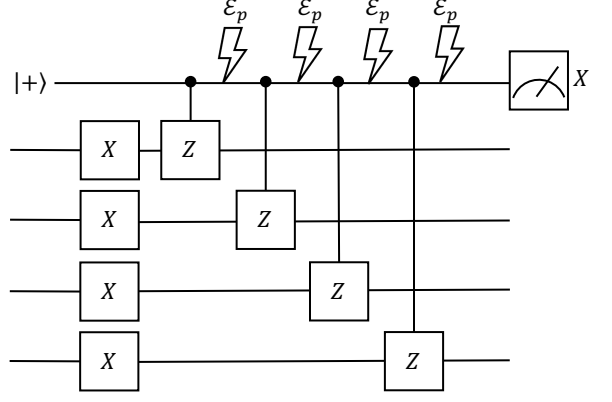


FIG. 6. Gate-based decomposition of the VQED gadget in Fig. 2 (b) for $[[4, 1, 2]]$ stabilizer code with $S_i = XXXX$ and $S_j = ZZZZ$. We assume that the single-qubit depolarizing noise $\mathcal{E}_p : \rho \mapsto (1-p)\rho + pI/2$ affects the ancilla qubit every time we perform controlled-Pauli gates.

and by uniformly sampling $i, j \in \{1, \dots, 2^{n-k}\}$ and taking the average of the distribution, we obtain

$$(1-p)^n \text{tr}[P\rho PO]. \quad (\text{A4})$$

Thus, even under the existence of noise on the ancilla qubit, we can still calculate the expectation value corresponding to the post-selected state ρ_{det} as

$$\text{tr}[\rho_{\text{det}} O] = \frac{(1-p)^n \text{tr}[P\rho PO]}{(1-p)^n \text{tr}[P\rho P]}. \quad (\text{A5})$$

In the same way, we can say that the value obtained through VQED in Eq. (17) remains unchanged even under the existence of such noise, since the numerator and the denominator of Eq. (17) are only multiplied by $(1-p)^{nL}$. The only change to the performance of VQED is the slight increase in the sampling overhead from $N = O(\varepsilon^{-2} \text{tr}[\rho'_{\text{det}}]^{-2})$ to $N = O(\varepsilon^{-2}(1-p)^{-2nL} \text{tr}[\rho'_{\text{det}}]^{-2})$.

The essential point of this robustness is that the noisy term $|0\rangle\langle 0| \otimes \rho''' + |1\rangle\langle 1| \otimes \rho''''$ in Eq. (A2) is removed when we take the expectation value of X for the ancilla qubit. We note that the same principle applies to other noise models that are not biased by Pauli X or Y , such as local dephasing and amplitude damping noise. We also note that the noise model we used for the VQED gadget in our numerical simulation is different from what we consider in this section: instead of assuming that the noise affects the ancilla qubits every after the execution of the controlled-Pauli gates, we assumed that the noise affects both the system and ancilla qubits every after the execution of S_i and controlled- S_j gates.

Appendix B: Transversal single-qubit gates in stabilizer codes

In this section, we clarify the sets of transversal single-qubit gates we use in the numerical simulation. For

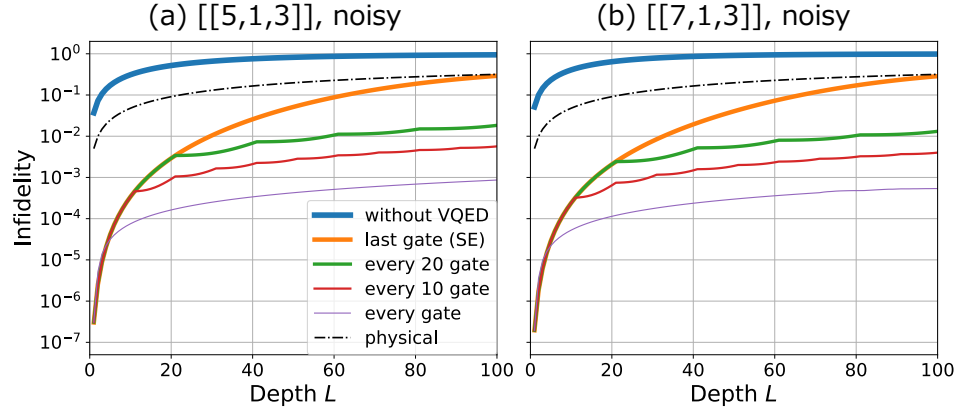


FIG. 7. Depth L dependence of infidelity $1 - \text{tr}[\rho_{\text{det}} |\bar{\Psi}\rangle\langle \bar{\Psi}|] = 1 - \langle \bar{\Psi} | \rho_{\text{det}} | \bar{\Psi} \rangle$ between the output state of the noisy circuit with VQED ρ_{det} and the noiseless circuit $|\bar{\Psi}\rangle$ for (a): $[[5, 1, 3]]$ and (b): $[[7, 1, 3]]$ stabilizer codes. All of the panels denote the results when the VQED gadgets are affected by local depolarizing noise. The “without VQED” line represents the infidelity when we did not perform VQED. The “last gate (SE)” line represents infidelity when we perform VQED only before the measurement, which is just a normal SE, as in Refs. [24, 25]. The “every 20 gates” and the “every 10 gates” lines represent infidelity when we perform VQED after every 20 and 10 gates. The “every gate” line represents infidelity when we perform VQED after every gate. The “physical” line represents the infidelity of a single physical qubit without encoding.

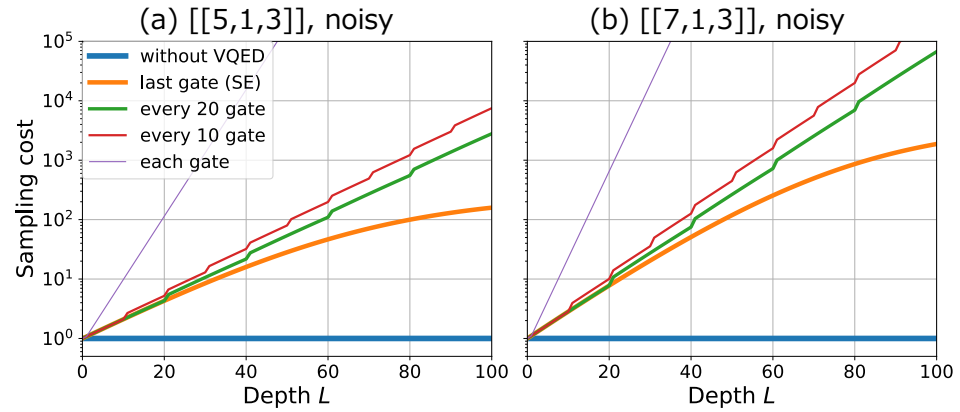


FIG. 8. Scaling of the sampling cost $\text{tr}[\rho'_{\text{det}}]^{-2}$ with respect to the depth L of the quantum circuit for (a): $[[5, 1, 3]]$ and (b): $[[7, 1, 3]]$ stabilizer codes. All of the panels denote the results when the VQED gadgets are affected by local depolarizing noise. The “without VQED” line represents sampling cost when we did not perform VQED. The “last gate (SE)” line represents sampling cost when we perform VQED only before the measurement, which is just a normal SE, as in Refs. [24, 25]. The “every 20 gates” and the “every 10 gates” lines represent the sampling cost when we perform VQED after every 20 and 10 gates. The “every gate” line represents the sampling cost when we perform VQED after every gate.

$[[4, 1, 2]]$ stabilizer code, we use a set of single-qubit Pauli gates as a set of transversal single-qubit gates [34]. For $[[5, 1, 3]]$ stabilizer code, we use $\{X, Y, Z, SH\}$ as a set of transversal single-qubit gates [29]. For $[[7, 1, 3]]$ stabilizer code, we use a set of single-qubit Clifford gates as a set of transversal single-qubit gates [29].

Appendix C: Numerical simulation of VQED when the VQED gadgets are noisy

In this section, we present the performance of VQED for $[[5, 1, 3]]$ and $[[7, 1, 3]]$ stabilizer codes when the VQED

gadget S_{i_l} gate and controlled- S_{j_l} gate in Fig. 3 are each affected by the local depolarizing noise $\mathcal{E}_p^{\otimes n}$ and $\mathcal{E}_p^{\otimes(n+1)}$ with the same error rate $p = 0.01$. Our results are shown in Fig. 7 and Fig. 8. The results for $[[5, 1, 3]]$ and $[[7, 1, 3]]$ stabilizer codes are qualitatively similar to those for the $[[4, 1, 2]]$ stabilizer codes shown in Fig. 4 (d) and Fig. 5 (d).